LAWRENCE
LIVERMORE
NATIONAL
LABORATORY

LLNL-CONF-549352

Visualizing Nuclear Scission Through a Multifield Extension ofTopological Analysis

D. Duke, H. Carr, A. Knoll, N. Schunck, H. A. Nam, A. Staszczak

April 17, 2012

VisWeek 2012
Seattle, WA, United States
October 14, 2012 through October 19, 2012

Disclaimer

Visualizing Nuclear Scission Through a Multifield Extension of Topological Analysis

David Duke, *Member, IEEE*, Hamish Carr, *Member, IEEE*, Aaron Knoll, Nicolas Schunck, Hai Ah Nam, and Andrzej Staszczak

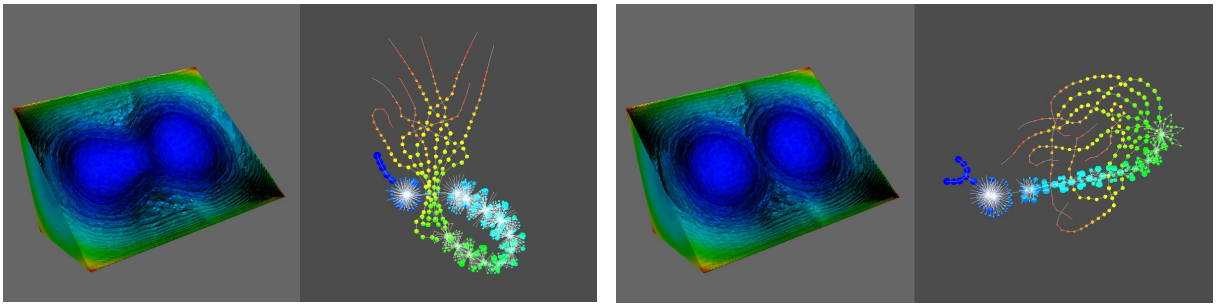

Fig. 1. Scission point: A single plutonium nucleus (left) breaks into two fragments (right). Each image shows the iso-interval slabs within the 3D domain, and the abstract structure of the underlying Joint Contour Net.

Abstract— In nuclear science, density functional theory (DFT) is a powerful tool to model the complex interactions within the atomic nucleus, and is the primary theoretical approach used by physicists seeking a better understanding of fission. However DFT simulations result in complex multivariate datasets in which it is difficult to locate the crucial 'scission' point at which one nucleus fragments into two, and to identify the precursors to scission. The Joint Contour Net (JCN) has recently been proposed as a new data structure for the topological analysis of multivariate scalar fields, analogous to the contour tree for univariate fields. This paper reports the analysis of DFT simulations using the JCN, the first application of the JCN technique to real data. It makes three contributions to visualization: (i) a set of practical methods for visualizing the JCN, (ii) new insight into the detection of nuclear scission, and (iii) an analysis of aesthetic criteria to drive further work on representing the JCN.

Index Terms—Topology, Scalar Fields, Multifields

1 Introduction

Problems in science, engineering and medicine rarely involve just one property of a system. Simulations of combustion, turbulence, seismic movements, meteorology, astrophysics, and molecular physics, all compute multiple properties simultaneously, such as temperature, pressure, velocity, vorticity, shear, combustion rate, and so on. To date, scientific visualization for such data has focused on techniques for representing *individual* properties. Visual exploration of multiple properties requires careful use of methods such as probing, glyphing, or multidimensional transfer functions. All of these approaches are ad hoc, relying on careful study and exploration to piece together a global understanding of the relationships from local, fragmented, models.

In physics, this problem is illustrated by many-body systems such as molecules, atoms or nuclei where the system as a whole is the product of very complex interactions among many constituents, the properties of which may not be very easily isolated. In this paper, we focus on nuclear fission, the process by which an atomic nucleus splits in two (or more) fragments. Although it was discovered more than 70 years ago, physicists are still working on a comprehensive description of this very complex phenomena rooted in the theory of the strong interaction rather than phenomenological models. Such a predictive power is needed for further insight in the formation of elements in the universe, but also to answer pressing societal questions related to energy production or stockpile stewardship. A particularly challenging aspect in the theory of fission is the ability to identify accurately, in a continuous $N-$dimensional manifold, the points where the original nucleus ceases to be whole, and where it is justified to introduce two separate density distributions corresponding to the fission fragments. This identification is conventionally done manually and relies on the physicists' intuition rather than clear mathematical arguments. By nature, however, this problem is an excellent candidate for multifield analysis.

Recent work [10] sets out a clear mathematical basis for multifield analysis: the Joint Contour Net (JCN). JCNs generalise the Contour Tree (and Reeb Graph) from one to an arbitrary number of scalar properties. Underlying this approach is a key assumption: that, by visualizing the JCN it will be possible to gain global insight into the relationship between the fields, and/or to identify important changes in the topological structure of the full system in terms of feature in the JCN. This has been demonstrated on small synthetic datasets, but not yet on real data linked to a specific scientific problem.

This paper makes two principal contributions:

1. We apply graph visualization tools to the JCN to analyse simulation data from nuclear physics, leading to new insight into the nuclear fission process, and a new general method for the future.
2. We demonstrate the utility of the JCN to real data, and explore the relationship between JCN analysis of multifields and contour tree analysis of single scalar fields.

- *David Duke and Hamish Carr are with the School of Computing, University of Leeds, UK, E-mail: {D.J.Duke, H.Carr}@leeds.ac.uk.*
- *Aaron Knoll is with Argonne National Laboratory, USA, E-mail: knoll@mcs.anl.gov.*
- *Hai Ah Nam is with Oak Ridge National Laboratory, USA, E-mail: namha@ornl.gov.*
- *Nicolas Schunck is with Lawrence Livermore National Laboratory, USA, E-mail: schunck1@llnl.gov.*
- *Andrzej Staszczak is with the Department of Theoretical Physics, University Marie Curie-Skłodowska, Lublin, Poland*

Manuscript received 31 March 2011; accepted 1 August 2011; posted online 23 October 2011; mailed on 14 October 2011.
For information on obtaining reprints of this article, please send email to: tvcg@computer.org.

The remainder of the paper is structured as follows. Section 2 describes nuclear density functional theory and its treatment of nuclear fission, then concludes with the key domain question addressed in this paper, namely finding the scission point in simulations of nuclear fission. These datasets are multivariate, and Sections 3 through 5 set out relevant formalisms and prior work including the JCN. Our visualization tools are described in Section 6: these include implementation of the JCN, and methods for drawing it. The subsequent two sections, 7 and 8, present our analyses of two substantial datasets. The first study, a simulation of fermium fission, serves to calibrate our approach. The second dataset, modeling fission in the plutonium nucleus, is more challenging, and our analysis contributes new insight into physicists' understanding of this system. Section 9 then reviews the contributions, and considers future research in this area.

2 Nuclear Fission in Density Functional Theory

Early models of fission were based on an empirical liquid-drop picture of the nucleus: fission occurs when one "stretches" the drop up to the point where it breaks in two [5]. Modern approaches aim at deriving an understanding of the fission process from the nucleon-nucleon interactions that make atomic nuclei possible. In this context, the major theoretical approach is nuclear Density Functional Theory (DFT) [3]. Its central assumption is that the complex many-body interactions of protons and neutrons within the nucleus can be hierarchized. In first approximation, everything happens as if all nucleons were moving independently of one another in some average quantum potential, the nuclear mean-field, which is computed, e.g., by convolving an effective two-body interaction with the density of nucleons. A mechanism named spontaneous symmetry breaking is invoked to deform the mean-field, introducing a first class of correlations in what would be otherwise a pure independent particle model. Beyond this first order approximation, corrections are required to account for quantum fluctuations but the mean-field approximation alone is surprisingly successful: it typically accounts for 99.9% of the atomic mass of elements, see for example [21, 22]. The DFT approach has three major advantages over its competitors: (i) it provides a simple yet rigorous framework based only on an interaction between nucleons, (ii) it only depends on a handful of free parameters, and (iii) it is the only computationally tractable approach of the structure of heavy nuclei.

Because fission involves 'stretching' the nucleus, the DFT treatment of the problem begins with identifying the relevant deformation degrees of freedom q of the mean-field. A realistic description of fission involves at least $N \geq 4$ degrees of freedom such as elongation, triaxiality, mass asymmetry, the degree of necking, etc. [32, 36]. The list of degrees of freedom defines what is called the collective space. The next task is to take a (not necessarily uniform) sample grid of this N-dimensional collective space and compute the total energy E at each point of this grid. As the dimensionality N of the collective space increases, the number of points may quickly become very large: high-performance computing is needed. The scalar field $E(q_1,\ldots,q_N)$ defines the potential energy surface (PES). At each point on the PES, the nucleus is characterized by properties such as the spatial density of protons and neutrons (scalar field $R^3 \to R$), the density of spin of each type of particles (vector fields $R^3 \to R^3$), etc. A given set of such properties is nothing but a particular realization of a multifield.

The PES themselves are the cornerstone of the microscopic theory of fission. They have some topology with a minimum at small deformations, the ground-state of the nucleus, together with secondary minima, ridges and valleys. Starting from the ground-state and following a path of least energy on the PES, we may observe at some point a discontinuity with a sharp drop of the energy: this is the scission point, and it defines the moment where the nucleus fragments and can not be considered as whole any longer. Often, the identification of the scission point is obvious, cf. for example the so-called asymmetric elongated fission path (aEF) of the fermium isotopes in figure 4. However, there are also many cases where it is much more ambiguous. In figure 4, the pathway labeled sCF (as symmetric compact fission) does not show any marked discontinuity. The definition of the scission point in this case is very arbitrary, yet it is clear that for the collective variable $q \equiv Q_{20}$ such that $q > 250$ b, the system has split in two fragments. In fact, even in the simplest cases where a discontinuity in the N-dimensional PES is clearly visible, it is almost always possible to enlarge the collective space by adding one or a few collective variables that will remove this discontinuity, and, as a consequence, blur the identification of the scission point. This local enlargement of the collective space and its consequence on the scission point is illustrated in figure 8 for the plutonium isotope.

There are many other cases where rigorous multifield analysis techniques could prove very valuable for nuclear physicists. For example, the description of neutron-induced fission, e.g. in nuclear reactors requires adding thermal effects to the theory. A theoretically unpleasant consequence of having to deal with a nuclear temperature is that nucleons tend to be more and more delocalized: densities extend further outside the nucleus. As a consequence, the definition of the scission point becomes more and more ambiguous, if not questionable. Apart from the identification of the scission point itself, perhaps as important is the detection of the nascent pre-fragments in the fissioning nucleus [30, 31, 37]. This is the signal that global degrees of freedom associated with the whole nucleus may have to be replaced by individual degrees of freedom for each fragment. Yet, there is currently no systematic way to perform this switch from global to local degrees of freedom, and multifield analysis offers an appealing option.

Since the task involves detection of a particular combinatorial event between distinct objects encoded in a multi-field composed of multiple scalar fields, this problem is well-suited to topological analysis. Thus, in order to identify the scission points, we must first discuss the principles of topological analysis and visualization in the scalar case, then discuss multifield visualization and in particular the extension of topological analysis to multifield data.

3 Scalar Topological Analysis

In recent years, topological analysis has increasingly been applied to the analysis, visualization and comprehension of scientific data sets [7]. Two complementary approaches have been developed - contour-based analysis [12] and gradient-based analysis [16]. Of these, contour-based analysis detects objects and their relationships, while gradient-based analysis also detects regions of common behaviour. At the same time, contour-based analysis is computationally cheaper and simpler than gradient-based analysis: we therefore start with scalar topological analysis using the contour tree.

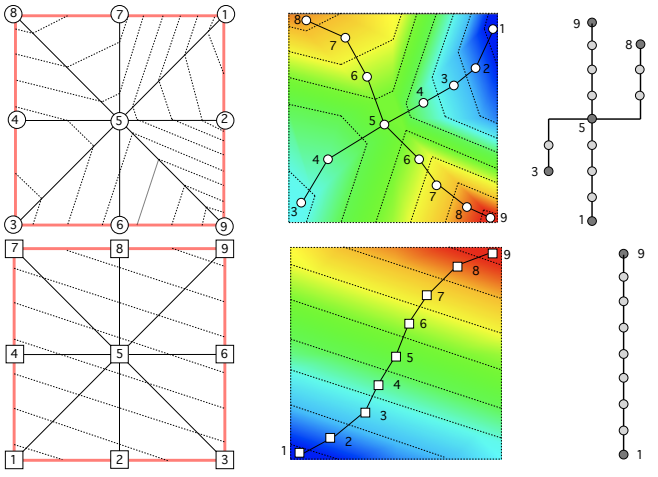

Fig. 2. A small multifield example. In the upper row, the first scalar field, with contours, slabs and contour tree. In the lower, the second scalar field, with contours, slabs and contour tree.

3.1 Contour Trees

Given a scalar field $f : M \subset R^m \to R$ over a manifold domain M, a level set $f^{-1}(h)$ is the pre-image of a given isovalue h, and a contour is a

single connected component of a level set. We note that each contour is (on standard assumptions) of one dimension lower than the original data set, because we have restricted it with respect to one variable.

In general, if we contract each contour to a single point, we obtain a graph called the Reeb graph [25]: when M is homeomorphic to a disk, the Reeb graph is a tree, and is called the contour tree [6]. more generally, this is called the Reeb graph when the domain of the function is a non-simple manifold. For scalar fields of the form an example of this is shown in Figure 2. In this figure, a small triangulated scalar field is shown with some contours (on the left), and a heat map to its right. Note that the contour tree captures the relationship between the maxima in red, the minima in blue, and the saddle point in the centre. All extrema are represented as leaf nodes and saddle points as interior nodes: all other points map to points on edges of the tree. Moreover, regions bounded by contours map to subsets of the tree, and branches of the tree therefore represent regions of the data.

The contour tree can be computed in $O(NlogN)$ time for triangulated scalar fields [11], and has been used for feature detection [12], volume rendering [35], and contour extraction [12].

3.2 Combinatorial Reduction

In computing contour trees and other topological abstractions of data, the first step is to establish a reduction of the input data to a combinatorial form, commonly a graph representation, over which algorithms can operate efficiently. This was initially done by making simplifying assumptions to fit the formal mathematics, but had the side effect of making computations more complex. In particular, the function was assumed to be defined over a triangulated (simplicial) mesh [2] with no two vertex isovalues identical [17], it is possible to reduce the computation to a combinatorial algorithm over the graph defined by the edges of the input mesh. Alternately, graphs can be defined directly from digital image connectivity rules [23].

More recently, Forman's Discrete Morse Theory [18] replaced gradient computation with a rigorous combinatorial approximation, allowing efficient approximation of the Morse-Smale Complex.

How data is reduced to graphs is therefore a key component of practical computational topology, and the most recent work in this area has shown an intimate link between quantization of data and contour properties. Initially, this research showed a linkage between computational statistics, geometric representations, and contours [8]. Later work added the role of the gradient in computing geometric properties [26], and extended it to improve direct visualisation of continuous multi-field data through scatterplots [1]. Most recently, histograms have been shown to compute measures of interval regions: regions given by equivalence under function value quantisation [13]. This implies that a combinatorial reduction for topological analysis can be based on contour quantization rather than simplicial reductions.

In summary, contour trees capture large-scale features of a scalar field by applying a combinatorial reduction to the input data, and algorithmically analysing the resultant graph. Since the scission problem involves a multifield (i.e. multiple scalar fields) instead, we must therefore turn our attention to existing multifield visualization methods and in particular the state of the art in multifield topological analysis.

4 Multifield Visualization

Compared to a scalar field, a multifield can be thought of as a collection of scalar fields with a shared domain or as a generalisation of a scalar field to a multi-dimensional range: $f : R^n \rightarrow R^m$. And, while R^n is usually taken to be Euclidean space, both R^m and R^n may in general be continous parameter spaces. For example, a record of temperature, pressure, and humidity over the surface of the Earth defines a function $f : R^2 \rightarrow R^3$, while a record of heat and gaseous concentration in a volumetric simulation of a plasma defines a function $f : R^3 \rightarrow R^2$. We will consider each of the samples in the data domain individually to be scalar functions, i.e. we do not address the case where observations explicitly include vector or tensor components.

We can construct a small running example by combining the scalar field from Figure 2 with a second scalar field on the same domain in Figure 2. If we combine the two to construct a function $f : R^2 \rightarrow R^2$, we instantly run into the major problem with multifield visualization: how to construct separate visual encodings for each field. Figure 3 illustrates this problem, with a heat map based on the sum of the two fields. Broadly speaking, multifield visualization is in its infancy, with methods that either reduce the multifield to a scalar field or map each element of the multifield to different visual channels.

5 Multifield Topological Analysis

As we have seen, successful tools have been developed for scalar topological analysis. It has been an open question, how to extend these tools to multifields, either by treating the properties as separate scalar fields, or by analysing the entire multifield at once. Moreover, recent work [13] has demonstrated that, for many purposes, quantized contours are a more appropriate form of analysis for the sampled and meshed data typical of scientific and engineering simulations. We therefore consider these three sets of research before proceeding.

Multiple Scalar Analysis: One approach has been to analyse each scalar field separately (e.g. in contour trees), then overlap the corresponding features to determine which features are simultaneously represented in two fields [28]. Extending this to more than two fields, however, results in defining a graph of relationships between features in the scalar fields, then searching for cliques representing large overlapping regions [27]. However, this approach only identifies features that are independently visible in each property.

Jacobi Sets: A second approach has been to generalise scalar topology to higher dimensions. A first step here was the introduction of Jacobi sets [14], which analyse the behaviour of critical points of one property on contours of another, but do not divide the domain of the function into regions of full dimension that identify features in the data. More recently, Reeb graphs were extended to Reeb spaces [15] for multifields, but efficient practical algorithms have been lacking, in part due to the complexity of the Reeb spaces.

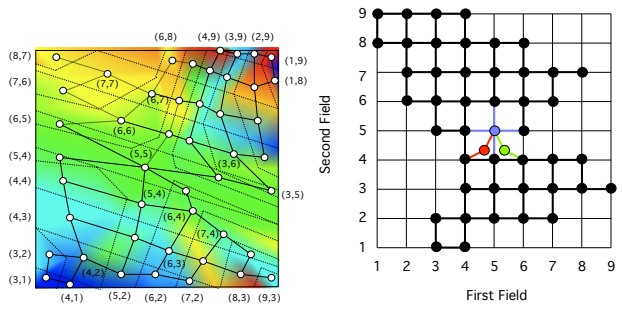

Fig. 3. Joint Contour Net for the small example. Left, the slabs after merging and the Joint Contour Net shown dual to the slabs. Right, range-space placement: isovalues are mapped to (x, y) as in the contour tree(Figure 2): where more than one node has a given isovalue, these are stacked perpendicular to the plane of the page (shown in colour).

Joint Contour Nets: Joint Contour Nets (JCN)s [9, 10] quantize the data domain into slabs in order to approximate Reeb spaces. Crucially, if the slabs for individual values are intersected, the result is still a slab of full dimension and with an easily defined neighbourhood. Figure 3 illustrates this quantisation: in this figure, the dotted lines indicate slab boundaries, where each slab has the property that all function values quantise identically. Note that there are no degenerate slabs, and that the dual graph of the slabs provides a combinatorial reduction for topological analysis.

If the dual graph is built up over many cells of the mesh, slabs in adjacent cells that have identical quantisations can be merged to reduce the complexity of the graph: the resulting mesh is called the Joint Contour Net, which can be thought of as a computational approximation (or tessellation) of the Reeb space of the multifield.

If we now look back at Figure 2, we can see that the Joint Contour Net for each individual property is simply the contour tree for that property, while for multifields, the Joint Contour Net captures all of the

topological relationships between properties, rather than the restricted information captured by Multiple Scalar Analysis or Jacobi Sets.

Given that the Joint Contour Net computation is explicitly based on quantizing the isovalues in the range of the function, we can vary the level of quantization as a crude method of simplifying the data and/or reducing the computational cost. For example, in Figure 2, the contour tree in the upper row can be computed correctly with slabs of size 2 rather than 1, while the contour tree in the lower row can be computed correctly with slabs of size 8. Similarly, in Figure 3, the key features of the Joint Contour Net show up with slabs of size 2.

6 Implementation

This section describes the architecture of the system used to carry apply multifield to the two fission datasets, and the techniques used for representing the resulting Joint Contour Nets.

6.1 Visualization Framework

A visualization pipeline was implemented in the Visualization Toolkit (VTK) [29], taking advantage of VTK's integrated support for both scivis techniques and information visualization. Version 5.8 of the toolkit was used, augmented by a small number of bespoke filters:

- A filter that extracts the JCN with the algorithm described in [9, 10]. This takes a simplicial mesh as input, and produces two outputs, (i) a graph dataset encoding the topological structure of the network, and (ii) a set of 3D polyhedra (or 2D polygons) stored as an unstructured grid, representing the slabs.
- A filter for converting the unstructured polyhedral cells into polygonal data that can be rendered.
- A filter for generating viewpoint-aligned ("billboard") glyphs that show, pointwise, the value of each component of a multi-scalar field. This filter is used in displaying the JCN, and is discussed in detail later in this section.

The JCN filter used in this paper was implemented as a testbed for multifield topology, and has not been optimized for performance. For example, it explicitly generates *all* of the isoslabs. While this capability was useful in the work reported here in relating the topological abstractions to the underlying physics, it is a significant performance bottleneck that will be addressed in subsequent work.

6.2 Drawing Joint Contour Nets

Trees and other networks from topological analysis are non-trivial for graph drawing. The (apparently) simple case of the contour tree is complicated as (a) the structure is an *unrooted* tree, and (b) in drawing the tree, there are often conflicting aesthetics – e.g. vertical positioning in 2D of nodes according to the isovalue of the corresponding contours, and horizontal positioning to reflect the branch hierarchy.

Two approaches to visualizing topological structure are (i) positioning nodes within the underlying manifold, or (ii) positioning the structure in a separate space (typically 2D or 3D euclidean space). Both approaches are illustrated in [24], which describes a layout for contour trees in 3D space inspired by orrerys. Layout in 2D space is more difficult; For layout in 2D [20] report an algorithm that uses heuristic search to reduce penalties arising from conflicting layout criteria. Neither of these approaches can be applied to the JCN, as both rely on structural properties of trees.

Absent a layout technique specialised to the structure of JCNs, we have identified three generic methods that provide complementary insights into their structure. Given a multifield function $f : R^n \rightarrow R^m$:

1. *Domain-space placement* positions each node at the centre of the slab in R^n to which it corresponds: an example of this can be seen in Figure 3. For $n \leq 3$, the resulting layout can be visualized directly; for $n > 3$ some form of dimensional scaling will be required. Although simple to compute a node position while building the JCN, in our experience it is difficult to discern features via this layout, and in particular difficult to identify combinatorial events within a sequence of JCNs.
2. *Range-space placement* positions nodes at the point in R^m defined by the threshold of the corresponding slab. This generalises the contour-tree drawing convention where CT node isovalue is mapped to one axis of the drawing space, and can be seen as a form of scatterplot, where samples in the data domain are connected by edges based on adjacency in the spatial domain.

   However, where two slabs have the same isovalue, the corresponding nodes will be co-located.
3. *Force-directed placement*: given the construction of the JCN from adjacent slabs, we expect these networks to have a mesh-like structure. Prior work [19] has shown that force-directed layouts can be effective for such graphs, and these algorithms avoid the problem of co-located vertices. Although there are issues of scalability for larger graphs, for the datasets used in this study force-directed placement was found to be practical.

Having placed the nodes, the next challenge is to relate nodes to the m-tuple of values for the corresponding slab. Our solution was a multi-variate glyph similar to pie glyphs [34], but adapted for multifield scalar data. Each glyph consists of a circle subdivided into m equal regions, each of which is then assigned a colour by mapping the corresponding component through a colour table.

The remaining difficulty was to relate nodes in the JCN to slabs in visualizations of the spatial domain. For analysis of DFT data, we do not need to make exact matches; our concern rather was to correlate features in the topological structure with regions of the data. As an expedient approach, we used the fact that the surfaces were subject to interpolation shading. For the surface of a slab defined by $(v_1, v_2, \ldots, v_m)$, we randomly assign one of the scalar values $\{v_1, v_2, \ldots, v_m\}$ to each vertex, and then pass the resulting single scalar field through a colour map. We make no claims that this is a perceptually good approach for multifield visualization in general, but for the specific task of identifying the scission point, it provided adequate support for relating the topological and spatial displays.

7 Fermium Dataset

Using the fermium-258 dataset with well defined fission pathways [32], the primary aim of the first study was calibration: whether the visualization tools reveal behaviour known *a priori* by the physicists to be present, allowing the visualization members of the team to tune visual representation, and simplifying the task of understanding how the structure of the JCN relates to underlying physical phenomena.

Three datasets, representing different trajectories through the energy landscape of the fermium nucleus, were provided by the physicists on the team for analysis. These were:

sCF : symmetric compact fission, representing the "simplest" form of fission, where the fermium nucleus splits fairly abruptly into two approximately equal nuclei, and

sEF : symmetric elongated fission, where the fermium nucleus elongates symmetrically, and

aEF : asymmetric elongated fission, where the fermium nucleus elongates asymmetrically, then a small group of nucleons breaks off to form a new nucleus.

Each dataset consisted of a trajectory in the higher-order parameter space defined by density functional theory, shown in Figure 4. As can be seen in this figure, the trajectory itself does not give a clear indication of whether or where scission occurs. Moreover, the conventional approach to detecting scission relies on computing overall energy for the system, and looking for evidence of a cusp at which scission occurs, as show in Figure 4. For example, while there is a clear jump in energy for aEF, the most that can be said for sCF is that there is a change in slope, and it is not clear exactly when scission occurs. Similarly, for sEF, there is a gradual decline in energy, but whether this corresponds to scission cannot be determined from this plot.

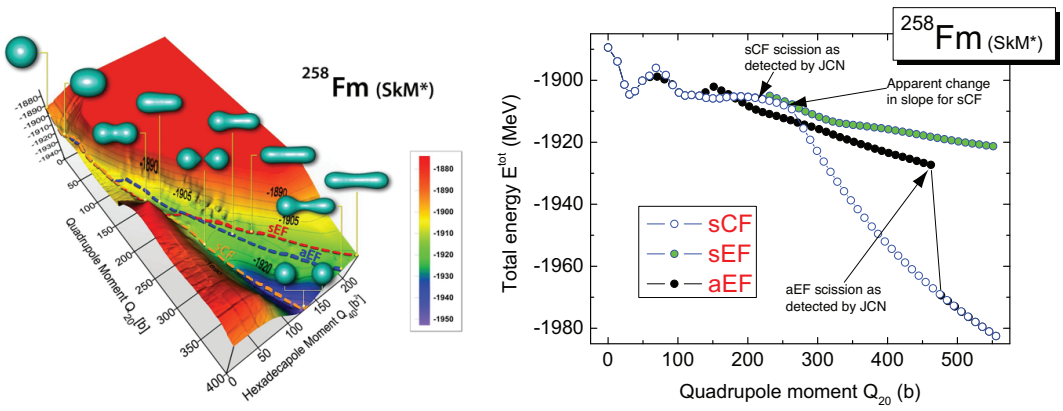

Fig. 4. Parameter space for fermium-258 fission (adapted from Bertsch et al. [4]). On the left, an energy landscape with three trajectories plotted and isosurface visualisations along each trajectory. On the right, energy plots along the specific trajectories studied (adapted from Staszczak et al. [33]). The JCN identified no scission in sEF, scission in aEF at the site marked, and scission in sCF several sites sooner than the energy plot would indicate.

For each of 56 sites along each of these trajectories, three scalar fields were sampled on a regular $19 \times 19 \times 19$ grid represented the positive, negative, and total field strength within the fermium nucleus as predicted by the model. Data for each field was provided in "raw" format: 8-bit unsigned integers. The three fields used in this and the subsequent plutonium study are:

p : spatial density of protons in the nucleus;

n : spatial density of neutrons;

t : spatial density of nucleons (protons and neutrons); $\rho_t(x,y,z) = \rho_n(x,y,z) + \rho_p(x,y,z)$

Of these, the sCF trajectory was analysed first. Figure 5 shows three snapshots from the initial analysis, at two levels of granularity.

Several things were immediately visible: the 'shell-like' arrangement of the slabs within the physical space, and the recurring star-like 'motifs' within the network are visible across all JCN images. Interpreting the shell-like structure in the 3D model is straightforward: field densities are highest at the centre of the dataset, and fall off towards the edge, taking the minimum value at the eight corner points. This interpretation is consistent with contour trees generated from the p/n fields individually, which display eight 'strands'. With respect to the star-like motifs, we noted the following:

1. The centre of the star corresponded to two high-degree nodes, most of whose neighbours were the low-degree nodes making up the remainder ('fringe') of the star.

2. Scaling glyphs according to slab triangle count showed that star centers corresponded to 'large' slabs, and fringes to small slabs.

Given the shell-like structure resulting from quantisation of the p/n fields, we hypothesised that these were the result of interference-like effects. Where a p-shell and an n-shell boundary were in close proximity, overlaps between the fields resulted in small regions where one or both of the field values crossed into the next slab interval; this structure is shown in Figure 6 (left). This was confirmed by taking a 2D slice through the data and colouring the field by slab-id. Figure 6(right) shows small slabs lying at the boundary between larger slabs (the degree-2 fringe nodes; the degree-1 nodes in the JCN 'fringe' are slabs that are fully contained within another).

With this understanding of the link between the JCN and underlying data, Figure 5 revealed further insight. The JCN images at sites 1 and 20 are suggestive of one chain of 'shells' with embedded fragments; the JCN in the third image however has a bifurcated structure.

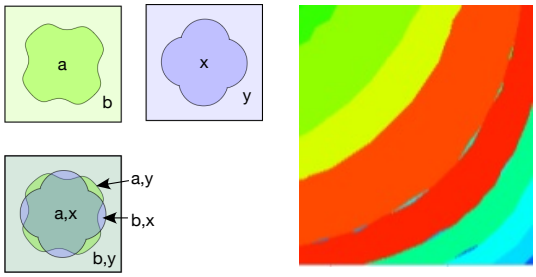

Fig. 6. Interpreting star-like motifs: (left) schematic of slab-edge boundaries, (right) 2D slice through dataset, coloured by slab identifier. Here a & b are the values of the first field defining its slab boundaries, while x & y are slab boundary values for the second field.

The colour mapping showed that the two 'ends' of the bifurcation corresponded to shells within the centre of the dataset, and inspection of these suggested the formation of two separate inner structure. Thus, the latter image corresponded to a point beyond scission.

To locate the scission point, we used scripts to generate MPEG video and/or JPEG image sets at each site along the given trajectory. Review of these outputs identified a significant topological shift at site 26: see Figure 7. This was proposed as the scission point, and subsequently confirmed by the physicists on the team. Notably, the scission is visible in the JCN on the trajectory *before* it shows up in the energy plot of Figure 4: again, the physicists confirmed that this was correct.

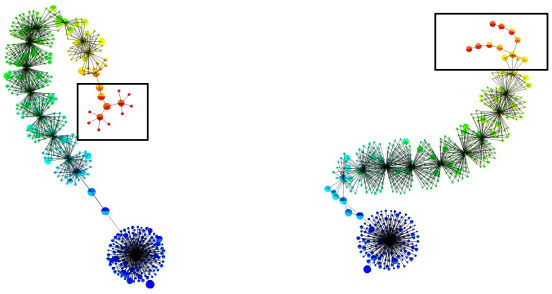

Fig. 7. Scission point in the sCF dataset. The tail of the dataset (site 25, left) has split into two clearly-defined strands in site 26 (right, in the arrowed box).

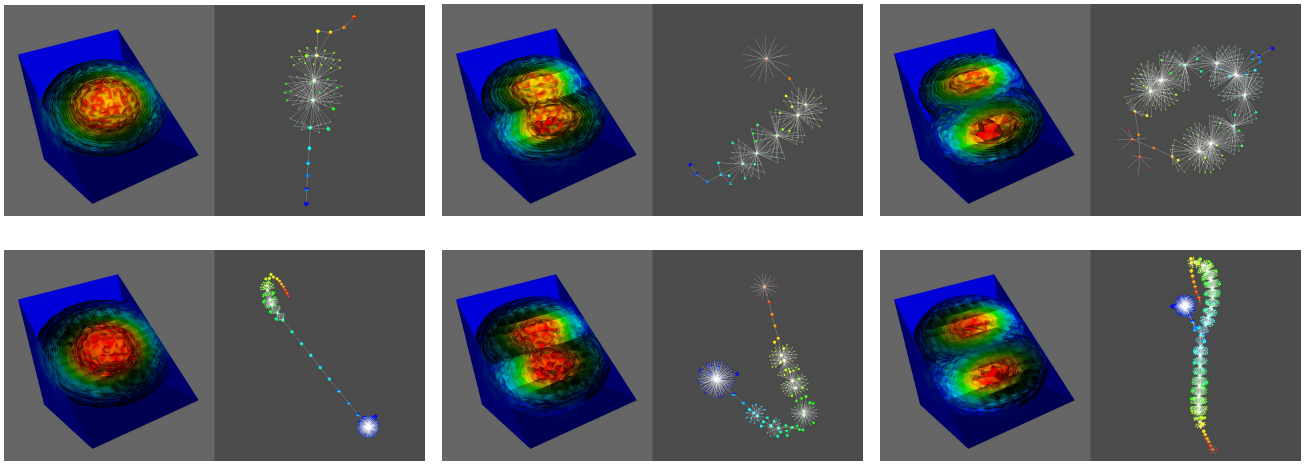

Fig. 5. JCN analysis of the sCF parameter trajectory. Top row at slab width 16, bottom row at slab width 8. Columns correspond to sites 1, 20 and 38 along the trajectory.

After seeing that the JCN worked for sCF, the physicists on the team provided two additional datasets (sEF and aEF). Again, the visualization members of the team were asked to identify the scission point.

In the aEF (Figure 8) trajectory, the JCN showed a clear bifurcation between sites 46 and 47, though with a precursor change between sites 44 and 45. The scission point was subsequently confirmed against the known model (see Figure 4).

In the sEF, initial analysis of the JCN at slab width 8 failed to identify a definite scission point, although changes in the 'backbone' of the structure suggested that fragments were organizing into discernible strands that could be precursors to fission. However, visual inspection at finer granularity (smaller slab width) still failed to identify any clear fission point, and this was reported to the physicists.

This was actually the correct conclusion to draw from the data: the physicists had deliberately posed sEF to see if the JCN would return a false positive. In fact, the sEF trajectory provided does not include a scission point, and the 'failure' to identify such a point via the JCN added further confidence in the utility of the multifield analysis.

8 Plutonium Dataset

The spontaneous fission of fermium nuclei confirmed the validity of the JCN to identify scission. We now consider plutonium (Pu) fission: abundant in the spent nuclear fuel generated by nuclear reactors, its properties have been the focus of numerous experiments. Physicists' understanding of its fission process is thus far more detailed than in the more exotic fermium superheavy element. Figure 8 shows the total energy of the nucleus as a function of its elongation Q_{20} from the ground-state (the first minimum, near $Q_{20} = 30$) to the scission point ('near' $Q_{20} = 345$, where energy drops suddenly) and beyond. For each point along the Q_{20} axis, the energy is taken as the minimum over three other dimensions in DFT, namely Q_{22}, Q_{30} and Q_{40}.

However, previous studies of fission of plutonium have shown that a four-dimensional collective space may not be enough in accurately reproducing the experimental data [36]. In the lower panel of the figure an extra degree of freedom, Q_N, is therefore considered. This additional collective variable is the number of particles in the neck, i.e. the integral over r, φ of the total density $\rho_t(r, \varphi, z)$ at the point z where the density is the lowest. What the lower panel of figure 8 shows is the energy at $Q_{20} = 345$ b as a function of Q_N, i.e., $\mathrm{Min}_{Q_{22},Q_{30},Q_{40}} E(Q_N; Q_{20} = 345)$. This value of Q_{20} is chosen just before the scission point as identified from the upper panel of the figure. The important consequence of adding the Q_N degree of freedom is that what was a discontinuity in a 4-d space (transition from $Q_{20} = 345$ to $Q_{20} = 346$ in the upper panel yields a 17 MeV energy loss) becomes a continuous path in a 5-d space, as evidenced in the lower panel of the figure. The only criterion that physicists could use to identify scission unambiguously, namely the discontinuity in the energy, has disappeared! Yet, study of the simulation shows that at $Q_N \geq 4$, the nucleus is whole, and at $Q_N \leq 0.1$, it has split in two fragments.

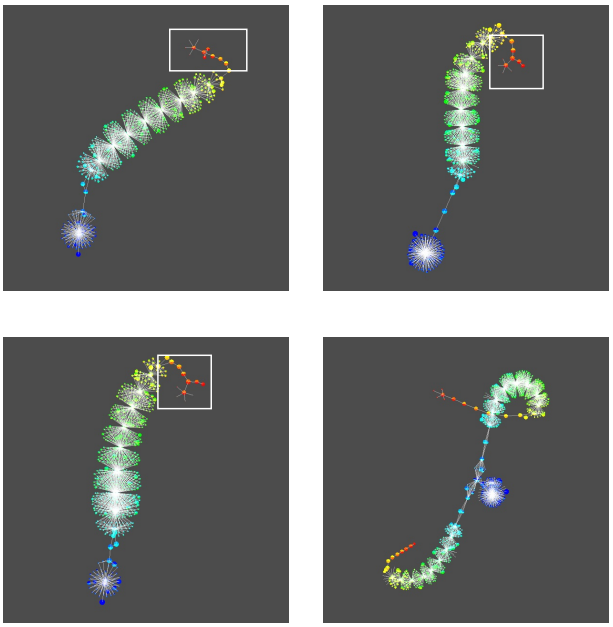

Fig. 8. Scission point in the aEF dataset. Starting from site 44 (top left), site 45 (top right) shows a break in local symmetry, persisting in site 46 (bottom right). Site 47 shows wholesale change, with the central 'spine' of the topology split into two branches.

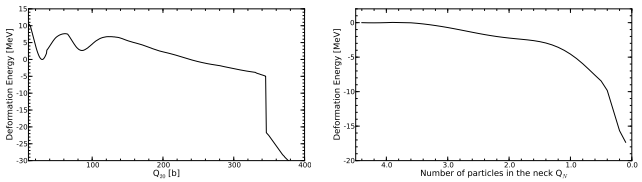

Fig. 9. Total energy of isotope ^{240}Pu as a function of quadrupole moment Q_{20} (left) and density of particles in the neck Q_N (right).

So, because models of Pu fission are more comprehensive, physi-

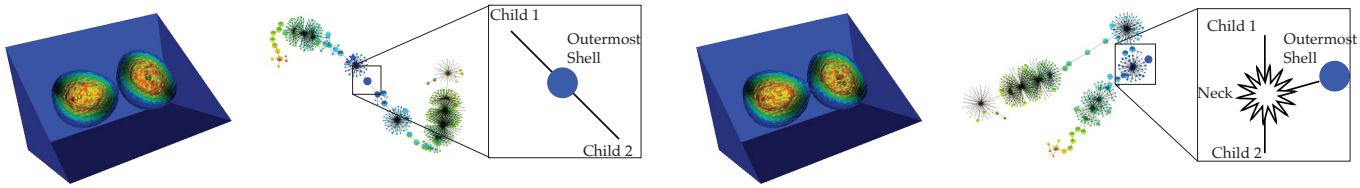

Fig. 10. Scission point in Q_N field. Left figure is post-scission ($Q_N = 0.4$), right figure is pre-scission ($Q_N = 0.5$)

cists face greater difficulty and uncertainty in interpreting the model and relating the higher-dimensional energy landscape to combinatorial changes in the underlying nuclear system. The goal of the second study, therefore, was (i) to use multifield analysis to locate the scission point along *both* the Q_{20} and Q_N axes of the Pu model, and (ii) to investigate whether the JCN analysis could shed light on the relationship between these fields and the structural changes within the Pu nucleus, e.g. identifying subtle differences in the behavior of neutron and proton density fields.

The initial analysis was performed on 669 sites sampled along the Q_{20} axis. As for fermium, each site along the trajectory corresponded to a 3-field (p, n, and t) volumetric dataset, in this case with dimensionality $40 \times 40 \times 66$. This data came from a different source to the fermium, and underwent pre-processing including negative log transformation, as there were concerns that the gradient in regions of the data would be problematic for JCN analysis. A consequence of the transformation used was that the sense of field density was changed, with the higher density regions mapping to lower values in the 8-bit fields. This inversion was eliminated from processing of later samples, but explains why the sense of the density field is flipped between Figure 8 and other images.

Analysis of these datasets was carried out with increasingly fine slab granularity. An initial sweep at slab width 32 failed to identify any combinatorial event, but sampling the datasets at resolution 16 showed a bifurcation appearing between sites 650 and 740; further analysis down to slab width 8 confirmed that the split appeared between sites 690 and 692 (Q_{20}=345). This transition is shown in Figure .

For Q_N, datasets were available for 45 sites along the trajectory in the second panel of Figure 8. A sweep through the data at resolution 8 indicated clearly a discrete point where the multifields topology underwent a significant change. Figure 10 shows the two sites (Q_N=0.4 and Q_N=0.5) on either side of the transition.

This putative scission point differs somewhat from that expected by the physicists (for example, scission was assumed to have occured at $Q_N \leq 1.0$ in [36]), but the situation is in fact more complicated. Figure 11 shows three further points along the Q_N trajectory, corresponding to $Q_N = 1.5$, 2.5, and 3.5. Each JCN has a branching structure: as the sequence progresses, the 'neck' becomes progressively larger. The event in Figure 10 is thus only the point where the neck disappears, leaving the density fields for two fragments enclosed only by the simulation bounds. This marks one end of a scission *region*, which starts when the bifurcation first appears. Although not sited along the given Q_N trajectory, such an event has already been identified, in Figure 8. *Thus, instead of simply identifying one combinatorial event representing scission, the JCN analysis has highlighted that scission itself is a process occupying a region within the energy space.*

The final point addressed is the relative utility of the JCN compared to contour trees of individual fields. Figure 12 shows contour trees for p and n fields and slab resolutions 16 and 8 for the sites at $Q_N = 0.4$ and 0.5 (either side of the end of the scission region). Although taken individually the contour trees are simpler, the different properties of protons and neutrons mean that neither field on its provides an unambiguous signal that the scission region has ended.

In fact, the 'quasi tree'-like structure of the fission JCNs (compared to the more general graph of the small example) reflects a feature of the underlying physics: the P and N fields are defined iteratively, and

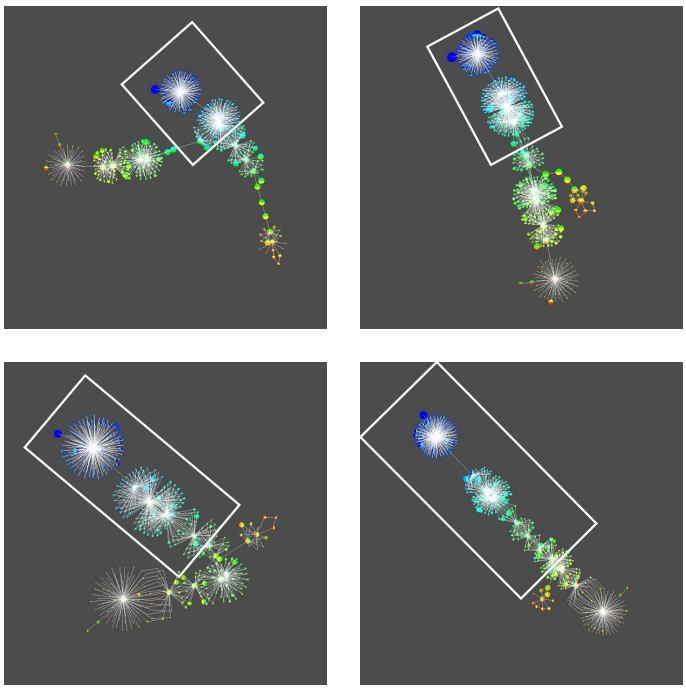

Fig. 11. Elongation of the neck region in the Joint Contour Net.

a scatterplot of the two fields show that the values occupy a comparatively narrow band within the data domain.

9 Conclusions

We set out with the intention to demonstrate the utility of JCN analysis in multifield data, and to provide visualization support for nuclear physicists in determining scission points in high-dimensional parameter spaces. In the outcome, we succeeded in showing that:

1. The JCN is an effective tool for studying nuclear fission parameter spaces,
2. The JCN gives a more precise answer than hitherto available to the fundamental question of when scission occurs, and in fact shows that scission does not necessarily occur at points of inflection in the energy plots,
3. Moreover, the JCN provides evidence that scission is best viewed as a *region* rather than a discrete point,
4. While the contour tree also answers this question, the JCN does so more reliably, and at lower levels of quantisation,
5. Star-like structures can be expected to occur in the JCN, but primarily represent aliasing at the boundary of quantization intervals, and can therefore be disregarded,

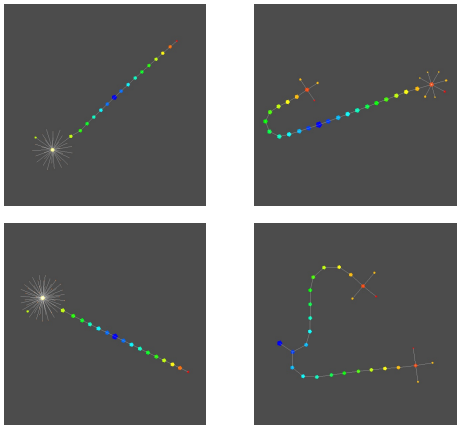

Fig. 12. Contour trees for the p (left column) and n (right column) fields around the Pu scission point. Top row: Q_N = 0.4; Bottom row: Q_N = 0.5.

In future, we intend to continue by considering forms of simplification and acceleration for JCN computation, improved algorithms for layout and visualization of the JCN, and exploring further uses of the JCN in nuclear physics. In particular, since the simulations come from wave-functions, particles may be localized in both fragments due to many-body quantum entanglement [37]. We believe that it may be possible to apply multifield techniques directly to the wave functions rather than to the total density of nucleons, and thus provide a criterion as to their degree of localization (left, right, everywhere).

Acknowledgments

This work was partly performed under the auspices of the U.S. Department of Energy by Lawrence Livermore National Laboratory under Contract DE-AC52-07NA27344, and by Oak Ridge National Laboratory under Contract DE-AC05-00OR22725 with UT-Battelle. Funding was also provided by the U.S. Department of Energy Office of Science, Nuclear Physics Program pursuant to Contract DE-AC52-07NA27344 Clause B-9999, Clause H-9999, and the American Recovery and Reinvestment Act, Pub. L. 111-5.

References

[1] S. Bachthaler and D. Weiskopf. Continuous scatterplots. *Trans. Vis. and Comp. Graph.*, 14(6):1428–1435, 2008.

[2] T. Banchoff. Critical points and curvature for embedded polyhedra. *J. Diff. Geom*, 1:245–256, 1967.

[3] M. Bender, P.-H. Heenen, and P.-G. Reinhard. Self-consistent mean-field models for nuclear structure. *Reviews of Modern Physics*, 75:121, 2003.

[4] G. Bertsch, D. DJ, and W. Nazarewicz. Computing atomic nuclei. *SciDAC Review*, Winter:42–51, 2007.

[5] N. Bohr and J. Wheeler. The mechanism of nuclear fission. *Physical Review*, 56:121, 1939.

[6] R. L. Boyell and H. Ruston. Hybrid Techniques for Real-time Radar Simulation. In *Proceedings of the 1963 Fall Joint Computer Conference*, pages 445–458. IEEE, 1963.

[7] P.-T. Bremer, G. Weber, V. Pascucci, M. S. Day, and J. Bell. Analyzing and Tracking Burning Structures in Lean Premixed Hydrogen Flames. *IEEE Transactions on Visualization and Computer Graphics*, 16(2):248–260, 2009.

[8] H. Carr, B. Duffy, and B. Denby. On histograms and isosurface statistics. *Trans. Vis. and Comp. Graph.*, 12(5):1259–1266, 2006.

[9] H. Carr and D. Duke. Joint contour nets: Topological analysis of mutlivariate data. In *VisWeek Poster Compendium*. IEEE, 2011.

[10] H. Carr and D. Duke. Joint contour nets: Topological analysis of mutlivariate data. In review at IEEE Transactions on Visualization and Computer Graphics, 2012.

[11] H. Carr, J. Snoeyink, and U. Axen. Computing Contour Trees in All Dimensions. *Computational Geometry: Theory and Applications*, 24(2):75–94, 2003.

[12] H. Carr, J. Snoeyink, and M. van de Panne. Flexible isosurfaces: Simplifying and displaying scalar topology using the contour tree. *Computational Geometry: Theory and Applications*, 43(1):42–58, 2010.

[13] B. Duffy, H. Carr, and T. Möller. Integrating Histograms and Isosurface Statistics. In review at IEEE Transactions on Visualization and Computer Graphics.

[14] H. Edelsbrunner and J. Harer. Jacobi Sets of Multiple Morse Functions. In *Foundations in Computational Mathematics*, pages 37–57, Cambridge, U.K., 2002. Cambridge University Press.

[15] H. Edelsbrunner, J. Harer, and A. Patel. Reeb spaces of piecewise linear mappings. In *Proceedings of the twenty-fourth annual symposium on Computational geometry*, pages 242–250. ACM Press, 2008.

[16] H. Edelsbrunner, J. Harer, and A. Zomorodian. Hierarchical Morse Complexes for Piecewise Linear 2-Manifolds. In *Proceedings, 17th ACM Symposium on Computational Geometry*, pages 70–79. ACM, 2001.

[17] H. Edelsbrunner and E. P. Mücke. Simulation of Simplicity: A technique to cope with degenerate cases in geometric algorithms. *ACM Transactions on Graphics*, 9(1):66–104, 1990.

[18] R. Forman. Discrete morse theory for cell complexes. *Advances in Mathematics*, 134:90–145, 1998.

[19] D. Harel and Y. Koren. Graph drawing by high-dimensional embedding. In *Graph Drawing*, volume 2528, pages 207–219. Springer-Verlag, 2002.

[20] C. Heine, D. Schneider, H. Carr, and G. Scheuermann. Drawing contour trees in the plane. *Trans. Vis. and Comp. Graph.*, 17(11):1599–1611, 2011.

[21] K. Kortelainen, T. Lesinski, J. Moré, W. Nazarewicz, J. Sarich, N. Schunck, M. Stoitsov, and S. Wild. Nuclear energy density optimization. *Physical Review C*, 82:24313, 2010.

[22] K. Kortelainen, J. McDonnell, W. Nazarewicz, P.-G. Reinhard, J. Sarich, N. Schunck, M. Stoitsov, and S. Wild. Nuclear energy density optimization: Large deformations. *Physical Review C*, 85:024304, 2012.

[23] S. Mizuta and T. Matsuda. Description of the topological structure of digital images by region-based contour tree and its application. *IEIC Technical Report (Institute of Electronics, Information and Communication Engineers)*, 104(290):157–164, 2004.

[24] V. Pascucci, K. Cole-McLaughlin, and G. Scorzelli. Multi-resolution computation and presentation of contour trees. In *Proc. Visualization, Imaging, and Image Processing*, pages 452–290. IASTED, 2004.

[25] G. Reeb. Sur les points singuliers d'une forme de Pfaff complètement intégrable ou d'une fonction numérique. *Comptes Rendus de l'Acadèmie des Sciences de Paris*, 222:847–849, 1946.

[26] C. Scheidegger, J. Schreiner, B. Duffy, H. Carr, and C. Silva. Revisiting histograms and isosurface statistics. *Trans. Vis. and Comp. Graph.*, 14(6):1659–1666, 2008.

[27] D. Schneider, C. Heine, H. Carr, and G. Scheuermann. Interactive Comparison of Multifield Scalar Data Based on Largest Contours. *Accepted to Computer-Aided Geometric Design*, 2012.

[28] D. Schneider, A. Wiebel, H. Carr, M. Hlawitschka, and G. Scheuermann. Interactive Comparison of Scalar Fields Based on Largest Contours with Applications to Flow Visualization. *IEEE Transactions on Visualization and Computer Graphics*, 14(6):1475–1482, 2008.

[29] W. Schroeder, K. Martin, and B. Lorensen. *The Visualization Toolkit: An Object-Oriented Approach to 3D Graphics*. Kitware, 2006.

[30] J. Skalski. Relative kinetic energy correction to self-consistent fission barriers. *Physics Review C*, 74(5):51601, 2006.

[31] J. Skalski. Relative motion correction for fission barriers. *Int. J. Modern Physics E*, 17:151, 2008.

[32] A. Staszczak, A. Baran, J. Dobaczewski, and W. Nazarewicz. Microscopic description of complex nuclear decay: Multimodal fission. *Physical Review C*, 80:14309, 2009.

[33] A. Staszczak, J. Dobaczewski, and W. Nazarewicz. Bimodal fission in the skyrme-hartree-fock approach. *Acta Physica Polonica*, B38:1589–1594, 2006.

[34] M. Ward and B. Lipchak. A visualization tool for exploratory analysis of cyclic multivariate data. *Metrika*, 51(1):27–37, 2000.

[35] G. Weber, S. Dillard, H. Carr, V. Pascucci, and B. Hamann. Topology-Controlled Volume Rendering. *IEEE Transactions on Visualization and Computer Graphics*, 13(2):330–341, March/April 2007.

[36] W. Younes and D. Gogny. Microscopic calculation of 240Pu scission with a finite-range effective force. *Physical Review C*, 80:54313, 2009.

[37] W. Younes and D. Gogny. Nuclear scission and quantum localization. *Physical Review Letters*, 107:132501, 2011.